ADVANCED ENERGY MATERIALS
www.advenergymat.de

Optically Switchable Smart Windows with Integrated Photovoltaic Devices

Hyun-Keun Kwon, Kyu-Tae Lee, Kahyun Hur, Sung Hwan Moon, Malik M. Quasim, Timothy D. Wilkinson, Ji-Young Han, Hyungduk Ko, Il-Ki Han, Byoungnam Park, Byoung Koun Min, Byeong-Kwon Ju, Stephen M. Morris, Richard H. Friend,* and Doo-Hyun Ko**

Smart windows with tunable optical transparency have been studied extensively for use as curtain-free windows. A typical smart window is based on an electrochromic system, where external energy is required to switch between the transparent and opaque states. Here, a new design for a smart window is presented incorporating an optically tunable liquid-crystal layer with a transparent solar cell. Depending on the incident light, the device switches from a transparent, energy-harvesting mode (day mode) to an opaque, idle mode (night mode).

Switchable optical materials have attracted considerable attention because of their broad application in the building environment, vehicle windows, and sunroofs. The technologies under development for switchable windows are broadly categorized by the materials that are used. Specifically, these include electrochromic materials, liquid crystals (LCs) and electrophoretic/suspended-particle devices, each technology with its own unique characteristics and advantages.[1] Electrochromic windows take advantage of materials with transparency that can be modulated with the application of an electric field, and the change in the optical properties is controlled by switching between an oxidized and a reduced form of the electroactive layer.[2] LC-based devices, on the other hand, often involve a dye guest-host effect whereby the absorption properties of the dye are altered by the reorientation of the liquid crystalline molecules with an applied electric field.[3] In addition to electric fields, the illumination with light that has specific wavelengths can also change the device transparency by utilizing optically switchable LCs. This is highly beneficial for smart window applications because the window automatically changes its configuration from a transparent to an opaque state depending upon the ambient light conditions.

In addition to switching between transparent and dark state, other functionalities can be integrated to create "smarter" windows, for example, in the form of energy harvesting.[4] Recently, there has been significant research on materials for photovoltaic devices, methods for controlling the morphology of such materials, and optimization of the device geometry. This combined research has resulted in high efficiency photovoltaic (PV) devices with efficiencies greater than 10%.[5] Along with the pursuit of high efficiency devices, different approaches have been proposed to find elegant solutions to the integration of PV devices such as building-integrated photovoltaics (BIPV), whereby a visibly transparent PV is employed as a means to harness the incident solar spectrum for energy conversion.[6] Combining a transparent PV device with a photoresponsive window, which enables automatic transition from opaque to transparent state depending upon ambient conditions, is a promising approach for the smart window. Such a window would be able to generate power during daytime and would then act as a shutter during the night for added privacy. Moreover this photoreaction should be reversible and function without any consumption of power. Here, we demonstrate an optically switchable smart window system that incorporates a photovoltaic layer into a photoresponsive LC device. Combination of these two structures offers numerous unprecedented advantages over conventional window designs.

An optically switchable chiral nematic LC is selected to provide a high contrast optical shutter that can be formed by sandwiching a photoresponsive short-pitch chiral nematic between

H.-K. Kwon, K.-T. Lee, Dr. K. Hur, S. H. Moon, J.-Y. Han, Dr. H. Ko, Dr. I.-K. Han, Dr. B. K. Min, Dr. D.-H. Ko
Korea Institute of Science and Technology
Hwarangno 14-gil
Seongbuk-gu, Seoul 136–791, Republic of Korea
E-mail: dhko@kist.re.kr
H.-K. Kwon, K.-T. Lee, Prof. B.-K. Ju
College of Engineering
Korea University Anam-ro, Seongbuk-gu
Seoul 136–713, Republic of Korea
Prof. B. Park
Department of Materials Science and Engineering
Hongik University
72–1, Sangsu-dong
Mapo-gu, Seoul 121–791, Republic of Korea
Dr. M. M. Quasim, Prof. T. D. Wilkinson
Centre of Molecular Materials for Photonics and Electronics
Department of Engineering
University of Cambridge
9 JJ Thomson Avenue
Cambridge CB3 0FA, UK
Prof. S. M. Morris
Department of Engineering Science
University of Oxford
Parks Road, Oxford OX1 3PJ, UK
E-mail: stephen.morris@eng.ox.ac.uk
Prof. R. H. Friend
Cavendish Laboratory
Department of Physics
University of Cambridge
J. J. Thomson Avenue
Cambridge CB3 0HE, UK
E-mail: rhf10@cam.ac.uk

DOI: 10.1002/aenm.201401347

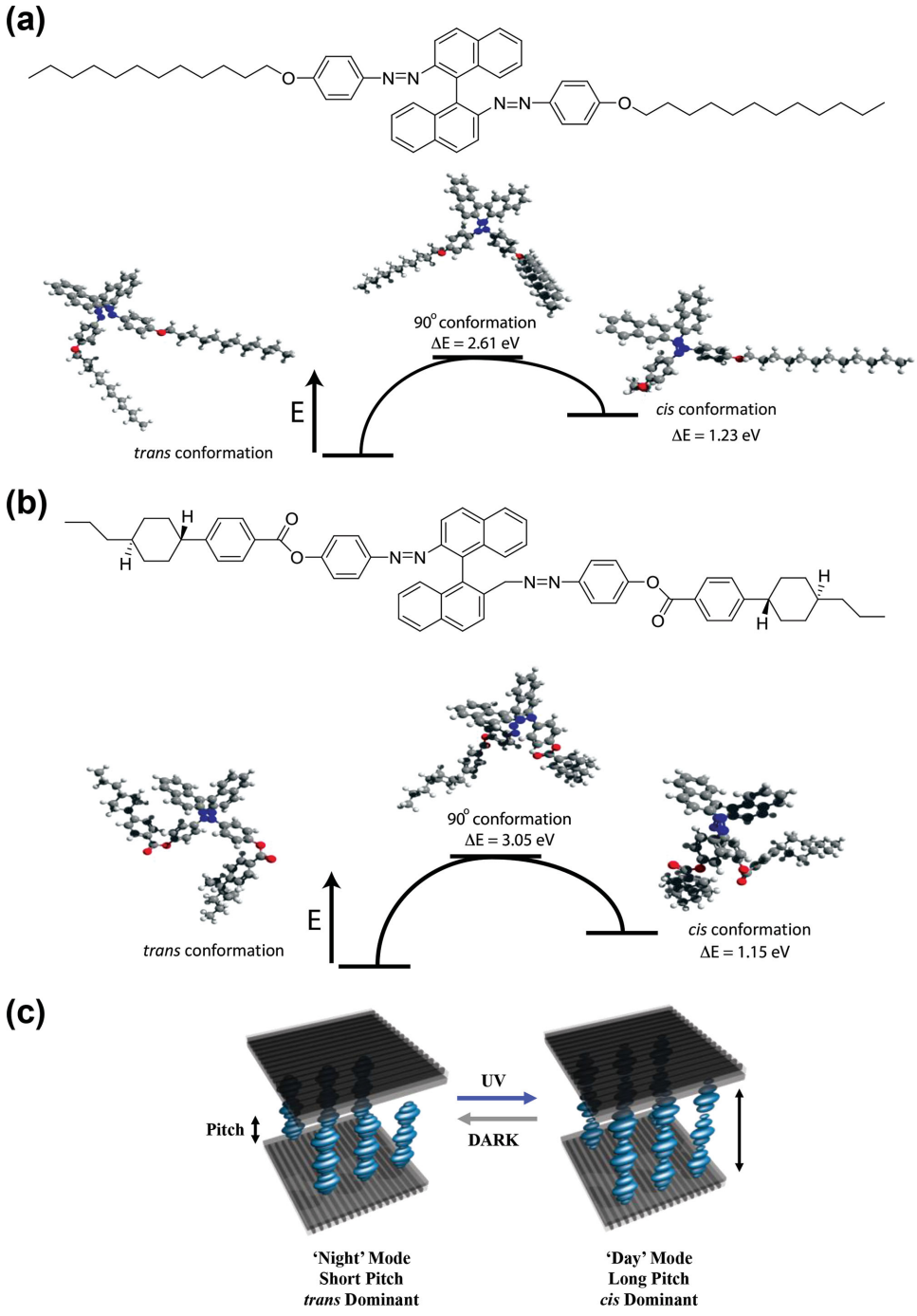

Figure 1. a,b) Molecular structures for the two photo-responsive bis (azo) dopants along with the DFT simulation results showing transition from trans to cis conformation through a 90° conformation. c) Schematic illustration of the photoresponsive LC device.

crossed polarizers.[7] In this case, the pitch of the chiral nematic LC is sufficiently short such that when the LC material is filled into a pair of anti-parallel rubbed polyimide glass cells whereby the axis of the helix is parallel to the surface normal, the device appears dark between crossed polarizers. This short-pitch chiral nematic mixture is doped with photoresponsive chiral bis (azo) dopants that enable the pitch to be extended when subject to UV light. The bis (azo) photoresponsive materials were chosen due to various advantages including thermal stability and wide optical tuning range.[8] In particular, these bis (azo) chiral dopants undergo trans to cis configuration change triggered by UV light, and vice versa in the dark.

With these benefits, two dopants in particular have been selected in this study to fabricate photo-responsive LC device, and molecular structures and calculated cis-trans conformation of the two dopants are shown in **Figure 1**a,b. In molecular structures, the long alkyl chain of the molecule (a) offers more conformational freedom and higher solubility in the nematic

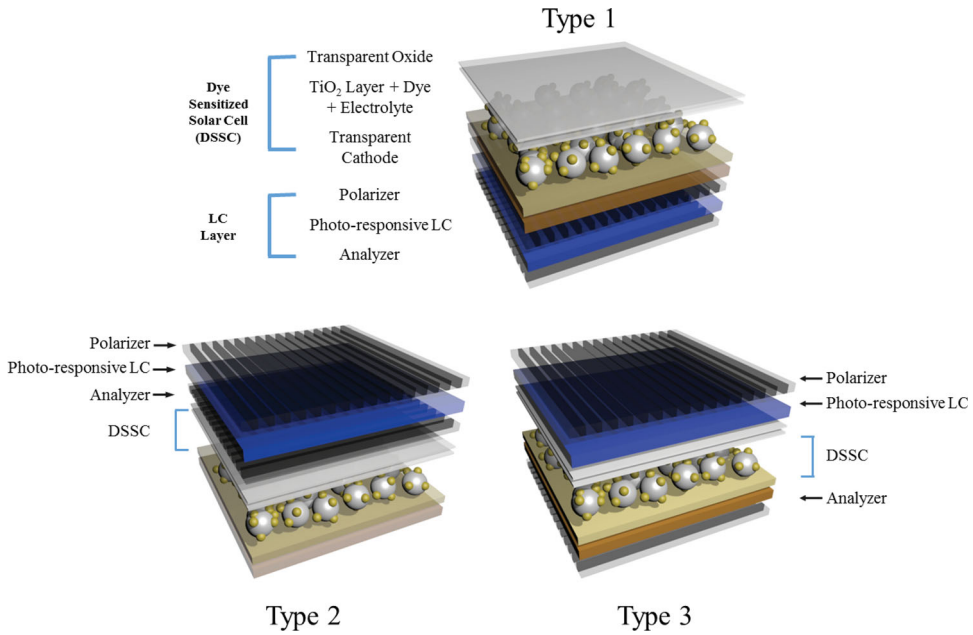

Figure 2. Schematics of the dye-sensitized solar cell with an optically responsive shutter for three different device configurations. Type 1 arrangement has a semitransparent solar cell on top of an optically switchable LC layer. On the other hand, for Type 2 the LC layer is stacked on top of a photovoltaic layer and for Type 3 the LC and PV layers are sandwiched between the polarizer and analyzer.

host than molecule (b) because the relatively bulky rigid end group in molecule (b) causes higher steric hindrance. In order to identify the energy profile of cis-trans isomerization of our dopant molecules we performed ab initio calculations using a popular density functional theory (DFT) package, Q-CHEM, with a B3LYP exchange functional and 6–31G** basis set.[9] The molecular structures were fully relaxed by minimizing their potential energies while fixing the torsional angle of azo group. Multiple initial configurations at each torsional angle were utilized in order to rule out existing metastable states of large dopant molecules, 132 atoms for compound (a) and 134 atoms for compound (b). The calculation reveals that the cis-trans conformation would be isomerized through transient status described as the 90° conformation, corresponding to the highest potential energy, and trans conformations for both materials are more favorable than cis configurations. In particular, compound (a) is expected to favor relatively facile formation change from trans to cis by external driving force (i.e., UV exposure) due to relatively low transition state energy between the trans and 90° conformations. On the other hand, the higher energy barrier of compound (b) implies that the trans conformation is conserved even under UV exposure. In essence, this conservation of trans conformation assists and accelerates recovery to initial-state of chiral LCs under UV free condition.

Here, the 10:1 ratio of the two molecules is mixed with a photo-insensitive chiral dopant and is dispersed into the nematic host E7 (Merck KGaA). Without UV exposure, the dominant trans-isomers, with the highest twisting power, decreases the pitch and results in blocking of the light by crossed polarizers. In the presence of UV (e.g., wavelengths below 400 nm), the twisting power of chiral dopants decrease for cis-trans isomerization and as a result, the pitch of the LC device extends and light is transmitted through the crossed polarizers. This process can be repeated through controlling the UV exposure. A schematic illustration of the photoresponsive LC device is shown in Figure 1c.

Our smart window was realized by combining an optically tunable LC layer with a dye sensitized solar cell (DSSC). Depending upon the application, a variety of device configurations are possible, as shown in **Figure 2**: one approach is that the LC cell can be placed underneath the DSSC (Type 1). In this case, a relatively higher power generation can be expected because the incident light would be fully harnessed by the DSSC without losses through the LC layer (e.g., polarizer). Second, the LC layer could be stacked on top of the DSSC (Type 2). The incident light is then transmitted through the LC layer prior to the DSSC, although the transmittance of incident light would be lower due to losses associated with the LC layer. In Type 3, the DSSC and the LC layer is sandwiched between the crossed polarizers. In this structure, the polarized beam through the DSSC would be regulated by the LC cell and the analyzer. Recent progress on polarizable organic PVs has opened up the possibility to modulate light polarization through PV devices, and this configuration may offer no loss of photocurrent due to the polarizers.[10] All these structures would be a possible scenario for the smart window applications, and we consider all three in this study.

For the photovoltaic component, we have selected a DSSC primarily for its semi-transparent and versatile properties. Moreover, a vacuum-free process combined with abundant material allows comparatively less expensive production and high scalability compared to conventional silicon solar cells.[11] Our DSSC is composed of a nanoporous titanium dioxide (TiO_2) layer loaded with dye, a Pt electrode, and an electrolyte layer for the oxidation/reduction reaction. Compared to thin-film Si-based solar cells, DSSCs offer a greater transmittance,

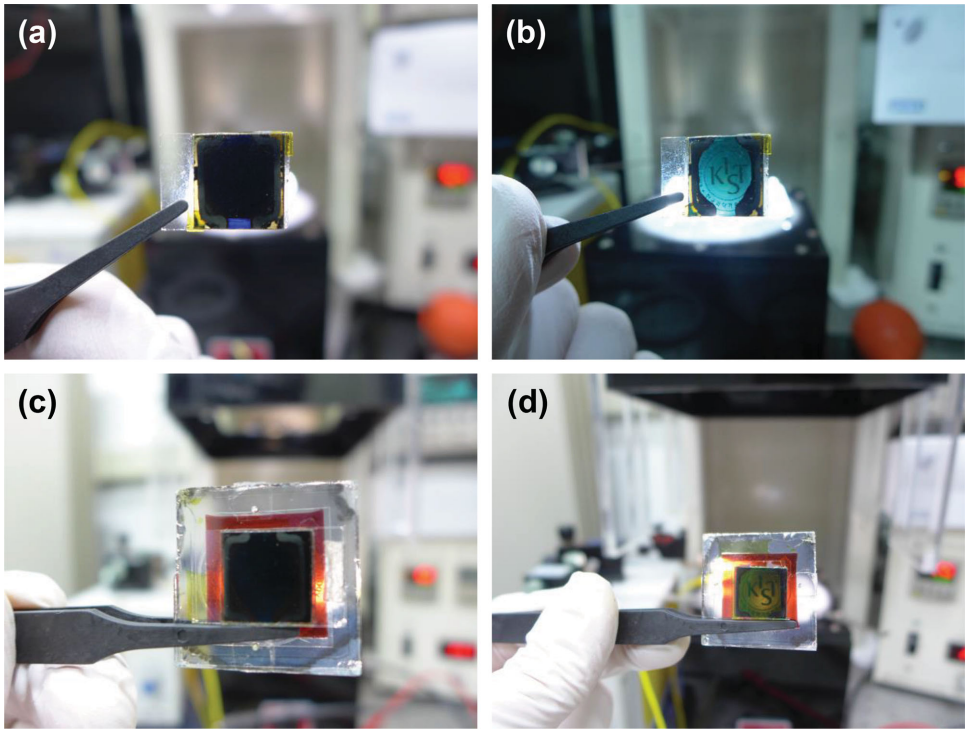

Figure 3. Photographs of the optically tunable photovoltaic smart window. a,b) The phototunable LC device alone in the dark and transparent states, respectively. c,d) The integrated device with the photovoltaic layer underneath the LC layer (Type 2). In (a,c), a 390 nm UV cut-off filter was used to show that the LC layer remains in dark state without a UV source. Removing the UV filter, the LC layer switched to a transparent state under exposure of 1 sun condition for 60 s as shown in (b,d).

primarily determined by the device structure, cathode thickness, and dye molecule concentration.[12] The dye in the DSSC governs the absorption spectrum thus giving flexibility of our choice for PV cells. Furthermore, careful selection of the dye can also enhance the window's performance in conjunction with the optically tunable LC layer. In this particular device, the chiral nematic mixture has been designed to maximize transmission at wavelengths around 550 nm when exposed to UV radiation. This particular wavelength is optimal for absorption (near 510 nm) of the trimeric ruthenium complex dye used in the DSSC. In order to improve transmittance as a window, a semi-transparent (Pt) electrode is deposited.

Photographs of our device in the dark and transparent states with and without the DSSC are shown in **Figure 3**. An LC layer without the DSSC is shown in Figure 3a,b, in the dark and transparent states, respectively. The transparent state was achieved by exposing the device to a solar simulator (AM1.5G, 100 mW cm^{-2} 1 sun condition) for duration of 60 s. After UV exposure, the dominant isomer configuration becomes the cis-isomers and thus the chiral nematic has a relatively long pitch helix as previously discussed. When linearly polarized light from the first polarizer propagates along the longer-pitch chiral nematic, light is transformed into elliptically polarized light thus leading to transmission through the analyzer. In the transparent state, the haze observed in the device is caused by the anti-glare-type polarizer and this value can be controlled with the selection of other polarizers (see Supporting Information Figure S1 for the haze measurement of the film). The reverse transition from a transparent state to a dark state can be achieved with absence of UV light, as in the night time. Interestingly, our smart window system cannot be triggered by an indoor light source with relatively low UV intensity (see Supporting Information Figure S2 for LC opening threshold evaluation).

To quantitatively analyze the transmittance in both the dark and transparent states, a UV–Vis spectrometer was used. As shown in **Figure 4**b, light transmittance is enhanced around 550 nm where the dye, a trimeric ruthenium complex, in DSSC largely absorbed. This transmittance range is able to be tuned by concentration ratio of azo (bis) chiral dopants between compounds (a) and (b) (see Figure 1), which favors cis or trans isomers, respectively. The transmittance enhancement factor was calculated by measuring the transmittance of LC layer in day mode divided by the transmittance of night mode (both with polarizers). The integrated device with optimized optical performance is shown in Figure 3c,d with Type 2 configuration. Figure 3c shows the device in a dark state, with the minimum transmittance. This state can be considered as "night" mode, where the LC layer is in a dark state and the PV current is minimized. On the other hand, Figure 3d was obtained when the complete device was exposed to a solar simulator for 60 s to simulate day mode, with maximum transmittance and active PV current.

Figure 4a shows the *J–V* curve of the three different configurations considered here and the device performance is summarized in **Table 1**. As previously discussed, the LC layer can be situated in different positions depending on the application. Type 1, which consists of the DSSC on top of the LC layer, was found to have a short circuit current density (J_{sc}) of

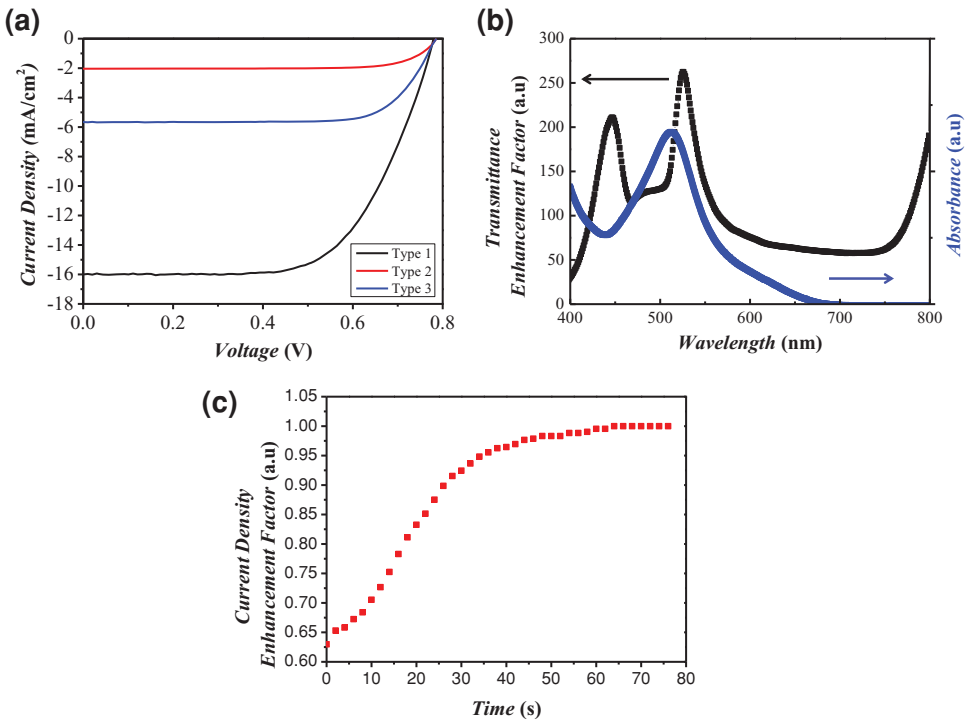

Figure 4. Characterization of the integrated smart window. a) *J–V* characteristics of three device types. b) Comparison of LC layer transmittance enhancement factor (with polarizers) and absorbance of trimetric dye in DSSC. c) Time–current density enhancement curve right after exposure of 1 sun condition.

16.43 mA cm^{-2}, an open circuit voltage (V_{oc}) of 0.744 V, a fill factor (*FF*) of 0.626, and an overall efficiency of 7.936% under 100 mW cm^{-2} 1 sun conditions. The Type 3 device, where the LC and solar cell are placed between the polarizer and analyzer, shows the following characteristics: J_{sc} of 5.671 mA cm^{-2}, V_{oc} of 0.779 V, fill factor of 0.745, and efficiency of 3.248%. This relatively low efficiency would be improved by incorporating light polarizing photovoltaics as discussed earlier.[10]

To investigate the effects of the LC layer on the DSSC, the Type 2 structure was further explored. For the Type 2 structure, only a dark photocurrent was recorded from PV device prior to 1 sun exposure because the very short pitch chiral nematic LC between the crossed polarizers blocks visible light from transmitting through the system. The pitch of the LC layer is then extended via exposure to 1 sun conditions and the device reaches the maximum transmittance. In this mode, the transmitted light reaches the DSSC and is converted into electrical energy with the following characteristics: J_{sc}, V_{oc}, *FF* and efficiency were recorded to be 2.13 mA cm^{-2}, 0.698 V, 0.739, and 1.099%, respectively. The relatively low efficiency compared with Types 1 and 3 mainly originates from the optical loss, which is primarily due to the polarizers.

Table 1. Photovoltaic performance for three types of smart window configurations.

Structure	Efficiency [%]	J_{sc} [mA cm^{-2}]	V_{oc} [V]	Fill factor [%]
Type 1	7.963	16.43	0.774	0.626
Type 2	1.099	2.13	0.698	0.739
Type 3	3.248	5.671	0.779	0.745

To confirm the device stays in night mode without UV element, a 395 nm cut-off long pass filter was used to block UV wavelength from the solar simulator. The LC layer remained in dark state and the device showed only dark photodiode behavior. Also transition from dark to day mode was tested as current density was evaluated in function of time. The 395 nm filter was removed from solar simulator and photocurrent was measured in interval of 2 s. Figure 4c shows change in the current density and the saturated current reveals the fast switching from night to day mode under 60 s.

In conclusion, we have demonstrated a novel smart window by combining an optically switchable LC shutter and a semi-transparent solar cell. The optically switchable LC shutter could be easily applied to many other types of transparent solar cells. Therefore, this approach clearly provides a versatile platform for BIPV devices. The operation in day mode collects solar energy with a sufficient transparency, while in night mode light is effectively cut off for privacy and security. The transition between these modes is achieved without any external power or signal.

Experimental Section

Preparation and Characterization of Samples: The 10:1 ratio of photoresponsive chiral bis (azo) dopants (see Figure 1b) synthesized by following previous report were mixed with a photo-insensitive chiral dopant R2011(Merck KGaA), and the mixture was dispersed into the

nematic host E7 (Merck KGaA).[7] The resultant chiral nematic LC mixture was filled into a 5μm-thick cell and sandwiched between two sheet polarizers that were crossed, which formed a dark state in the absence of UV light. For the DSSC fabrication, the N719 dyes and PMII (1-methyl-3-propylimidazolium iodide) were used as the dye and electrolyte, respectively, and the fabrication process was previously described in detail[13] A SAN-EI ELECTRIC solar simulator with a 300 W Xe lamp and an AM 1.5G filter was used to simulate the AM 1.5G solar spectrum. 100 mW cm^{-2} irradiation intensity was calibrated with a standard silicon solar cell. A Keithely 2400 equipment was incorporated to measure current densities. Controlling the optically tunable LC layer between dark and transparent states was done using the AM1.5 solar simulator with a λ = 395 nm cutoff UV filter (Newport). This system allowed for a cis–trans conformational change with 1 sun intensity. Without the UV element, the LC layer remained in a dark state, which was successfully tested using the UV filter. The transmittance was measured by a VARIAN 5000 UV–Vis Spectrophotometer. For haze measurements, haze spectrophotometry was measured with a Scinco HazeMate.

Supporting Information

Supporting Information is available from the Wiley Online Library or from the author.

Acknowledgements

This research was supported by the Pioneer Research Center Program through the National Research Foundation of Korea funded by the Ministry of Science, ICT and Future Planning (NRF-2013M3C1A3065040). It was also partially supported by a National Research Foundation of Korea Grant (NRF-2009-C1AAA001–0092935) funded by the Ministry of Science, ICT and Future Planning. D.H.K. acknowledges support from grant 2E25162 from a KIST project, and B.N.P. acknowledges support from the 2013 Hongik University research support fund.

Received: August 6, 2014
Revised: September 11, 2014
Published online:

[1] R. Baetensa, B. P. Jellea, A. Gustavsend, *Sol. Energy Mater. Sol. Cells* **2010**, *94*, 87.
[2] R. D. Rauh, *Electrochim. Acta* **1999**, *44*, 3165.
[3] a) L. Bouteillera, P. Le Barnya, *Liq. Cryst.* **1996**, *21*, 157; b) D. J. Gardiner, S. M. Morris, H. J. Coles, *Sol. Energy Mater. Sol. Cells* **2009**, *93*, 301.
[4] A. L. Dyer, R. H. Bulloch, Y. Zhou, B. Kippelen, J. R. Reynolds, F. Zhang, *Adv. Mater.* **2014**, *26*, 4895.
[5] a) L. Dou, J. You, J. Yang, C. Chen, Y. He, S. Murase, T. Moriaty, K. Emery, G. Li, Y. Yang, *Nat. Photonics* **2012**, *6*, 180; b) V. S. Gevaerts, A. Furlan, M. M. Wienk, M. Turbiez, R. A. J. Janssen, *Adv. Mater.* **2012**, *24*, 2130; c) M. K. Nazeeruddin, F. D. Angelis, S. Fantacci, A. Selloni, G. Viscardi, P. Liska, S. Ito, B. Takeru, M. Grätzel, *J. Am. Chem. Soc.* **2005**, *127*, 16835; d) L. Han, A. Islam, H. Chen, C. Malapaka, B. Chiranjeevi, S. Zhang, X. Yang, M. Yanagida, *Energy Environ. Sci.* **2012**, *5*, 6057; e) A. Yella, H.-W. Lee, H. N. Tsao, C. Yi, A. K. Chandiran, M. Nazeeruddin, E. W.-G. Diau, C.-Y. Yeh, S. M. Zakeeruddin, M. Grätzel, *Science* **2011**, *334*, 629.
[6] a) C.-C. Chen, L. Dou, R. Zhu, C.-H. Chung, T.-B. Song, Y. B. Zheng, S. Hawks, G. Li, P. S. Weiss, Y. Yang, *ACS Nano* **2012**, *6*, 7185; b) C.-C. Chen, L. Dou, J. Gao, W.-H. Chang, G. Li, Yang Yang, *Energy Environ. Sci.* **2013**, *6*, 2714; c) K. Zhang, C. Qin, X. Yang, A. Islam, S. Zhang, H. Chen, L. Han, *Adv. Energy Mater.* **2014**, DOI 10.1002/aenm.201301966; d) L.-P. Heiniger, P. G. O'Brien, N. Soheilnia, Y. Yang, N. P. Kherani, M. Gratzel, G. A. Ozin, N. Tétreault, *Adv. Mater.* **2013**, *25*, 5734; e) D. Colonna, S. Colodrero, H. Lindström, A. D. Carlo, H. Míguez, *Energy Environ. Sci.* **2012**, *5*, 8238; f) S. Yoon, S. Tak, J. Kim, Y. Jun, K. Kang, J. Park, *Build. Environ.* **2011**, *46*, 1899; f) G. E. Eperon, V. M. Burlakov, A. Goriely, H. J. Snaith, *ACS Nano* **2014***8*, 591; g) Y.-H. Chen, C.-W. Chen, Z.-Y. Huang, W.-C. Lin, L.-Y. Lin, F. Lin, K.-T. Wong, H.-W. Lin, *Adv. Mater.* **2014**, *26*, 1129; h) H.-W. Lin, Y.-H. Chen, Z.-Y. Huang, C.-W. Chen, L.-Y. Lin, F. Lin, K.-T- Wong, *Org. Electron.* **2012**, *13*, 1722.
[7] S. M. Morris, M. M. Qasim, K. T. Cheng, F. Castles, D.-H. Ko, D. J. Gardiner, S. Nosheen, T. D. Wilkinson, H. J. Coles, C. Burgess, L. Hill, *Appl. Phys. Lett.* **2013**, *103*, 101105.
[8] a) S. Kawata, Y. Kawata, *Chem. Rev.* **2000**, *100*, 1777; b) S. K. Yesodha, C. K. S. Pillai, N. Tsutsumi, *Prog. Polym. Sci.* **2004**, *29*, 45; c) H. Chi, K. Y. Mya, T. Lin, C. He, F. Wang, W. S. Chin, *New J. Chem.* **2013**, *37*, 735; d) Q. Li, L. Green, N. Venkataraman, I. Shiyanovskaya, A. Khan, A. Urbas, J. William Doane, *J. Am. Chem. Soc.* **2007**, *129*, 12908.
[9] Y. Shao, L. Fusti-Molnar, Y. Jung, J. Kussmann, C. Ochsenfeld, S. T. Brown, A. T. B. Gilbert, L. V. Slipchenko, S. V. Levchenko, D. P. O'Neill, R. A. Distasio Jr., R. C. Lochan, T. Wang, G. J. O. Beran, N. A. Besley, J. M. Herbert, C. Y. Lin, T. Van Voorhis, S. H. Chien, A. Sodt, R. P. Steele, V. A. Rassolov, P. E. Maslen, P. P. Korambath, R. D. Adamson, B. Austin, J. Baker, E. F. C. Byrd, H. Dachsel, R. J. Doerksen, A. Dreuw, B. D. Dunietz, A. D. Dutoi, T. R. Furlani, S. R. Gwaltney, A. Heyden, S. Hirata, C.-P. Hsu, G. Kedziora, R. Z. Khalliulin, P. Klunzinger, A. M. Lee, M. S. Lee, W. Liang, I. Lotan, N. Nair, B. Peters, E. I. Proynov, P. A. Pieniazek, Y. M. Rhee, J. Ritchie, E. Rosta, C. D. Sherrill, A. C. Simmonett, J. E. Subotnik, H. L. WoodcockIII, W. Zhang, A. T. Bell, A. K. Chakraborty, D. M. Chipman, F. J. Keil, A. Warshel, W. J. Hehre, H. F. Schaefer III, J. Kong, A. I. Krylov, P. M. W. Gill, M. Head-Gordon, *Phys. Chem. Chem. Phys.* **2006**, *8*, 3172.
[10] R. Zhu, A. Kumar, Y. Yang, *Adv. Mater.* **2011**, *23*, 4193.
[11] M. Grätzel, *J. Photochem. Photobiol. A: Chem.* **2004**, *164*, 3.
[12] M. Grätzel, *Acc. Chem. Res.* **2009**, *42*, 1788.
[13] a) S.-J. Park, K. Yoo, J.-Y. Kim, J. Y. Kim, D.-K. Lee, B. S. Kim, H. Kim, J. H. Kim, J. Cho, M. J. Ko, *ACS Nano* **2013**, *7*, 4050; b) H.-J. Koo, Ji. Park, B. Yoo, K. Yoo, K. Kim, N.-G. Park, *Inorg. Chim. Acta* **2008**, *361*, 677.